Author Manuscript

Author Manuscript

Author Manuscript

Author Manuscript

HHS Public Access

Author manuscript

Ultrasound Med Biol. Author manuscript; available in PMC 2021 September 01.

Published in final edited form as:

Ultrasound Med Biol. 2020 September ; 46(9): 2276–2286. doi:10.1016/j.ultrasmedbio.2020.05.010.

Tumor Vascular Networks Depicted in Contrast-Enhanced Ultrasound Images as a Predictor for Transarterial Chemoembolization Treatment Response

Ipek Oezdemir[1], **Corrine E. Wessner**[2], **Colette Shaw**[2], **John R. Eisenbrey**[2], **Kenneth Hoyt**[*,1]

[1]Department of Bioengineering, University of Texas at Dallas, Richardson, TX 75080

[2]Department of Radiology, Thomas Jefferson University, Philadelphia, PA 19144 USA

Abstract

Hepatocellular carcinoma (HCC) is prevalent worldwide. Among the various therapeutic options, transarterial chemoembolization (TACE) can be applied to the tumor vascular network by restricting the nutrients and oxygen supply to the tumor. Unique morphological properties of this network may provide predictive information about future therapeutic responses, which would be significant for decision making during treatment planning. The extraction of morphological features from the tumor vascular network depicted in abdominal contrast-enhanced ultrasound (CEUS) images faces several challenges, such as organ motion, limited resolution caused by clutter signal, and segmentation of the vascular structures at multiple scales. In this study, we present an image processing and analysis approach for the prediction of HCC response to TACE treatment using clinical CEUS images and known pathological responses. This method focuses on addressing the challenges of CEUS by incorporating a two-stage motion correction strategy, clutter signal removal, vessel enhancement at multiple scales, and machine learning for predictive modeling. The morphological features, namely, number of vessels (NV), number of bifurcations (NB), vessel to tissue ratio (VR), mean vessel length, tortuosity, and diameter from tumor architecture were quantified from CEUS images of 36 HCC patients before TACE treatment. Our analysis revealed that NV, NB, and VR are the dominant features for the prediction of long term TACE response. The model obtained an accuracy of 86% with a sensitivity and specificity of 89% and 82%, respectively. Reliable prediction of the TACE therapy response using CEUS-derived image features may help to provide personalized therapy planning, which will ultimately improve patient outcomes.

Keywords

contrast-enhanced ultrasound; hepatocellular carcinoma; transarterial chemoembolization; tumor vascular networks; machine learning

[*]Corresponding Author: Kenneth Hoyt (kenneth.hoyt@utdallas.edu), Kenneth Hoyt, PhD, MBA, FAIUM, University of Texas at Dallas, BSB 13.929, 800 W Campbell Rd, Richardson, TX 75080, Ph: (972) 883-4958.

Publisher's Disclaimer: This is a PDF file of an unedited manuscript that has been accepted for publication. As a service to our customers we are providing this early version of the manuscript. The manuscript will undergo copyediting, typesetting, and review of the resulting proof before it is published in its final form. Please note that during the production process errors may be discovered which could affect the content, and all legal disclaimers that apply to the journal pertain.

Author Manuscript Author Manuscript Author Manuscript Author Manuscript

Introduction

Hepatocellular carcinoma (HCC) is the fifth most prevalent cancer worldwide (Altekruse et al. 2009) and the third most common cause of cancer mortality (Kim and El-Serag 2019). Liver function and the tumor location and stage are considered when planning treatment options, such as surgical resection, transplantation, locoregional treatment, or systemic therapy (Brown et al. 2012). Patients with unresectable tumors are often candidates for a locoregional treatment option including drug-eluting bead transarterial chemoembolization (DEB-TACE or TACE) or transarterial radioembolization (TARE), which is not embolic. In the TACE procedure, polyvinyl alcohol beads or ethiodol are used to deliver chemotherapeutic agents into the tumor angiogenic network via a catheter placed in the tumor-feeding hepatic artery (Yamada et al. 1995). After the embolization, the beads start releasing the chemotherapeutic drug slowly into the tumor vasculature (Kloeckner et al. 2010). Successful treatment is defined by the complete occlusion of the tumor vasculature, but up to 65–75% of tumors show residual blood flow, and in this case, repeat TACE or alternative therapies are required (Shaw et al. 2015).

Monitoring TACE therapy response is performed with contrast-enhanced magnetic resonance imaging (CE-MRI) or with contrast-enhanced computed tomography (CECT) (Brown et al. 2012). The standard recommended time for the follow-up imaging is 4 to 6 weeks because both imaging modalities have limitations assessing the residual blood flow or lack thereof before this time point (Brown et al. 2012; Kloeckner et al. 2010; Shaw et al. 2015; Yan et al. 2002). Contrast-enhanced ultrasound (CEUS) is a low cost alternative to CECT and CE-MRI, and provides accurate evaluations of residual blood flow at 1 to 2 weeks post TACE treatment qualitatively (Shaw et al. 2015) and quantitatively (Averkiou et al. 2020; Nam et al. 2018). Quantifications of TACE therapy response using CEUS are performed with blood perfusion parameters that provide functional information about the blood flow dynamics after the TACE treatment.

Structural information from the architecture of the tumor angiogenic network can be characterized by their morphological features (Hoyt et al. 2015). These morphological features have also been shown as biomarkers for early response to anticancer therapy for different tumor models (Eisenbrey et al. 2011; Gessner et al. 2012; Ghosh et al. 2019; Hoyt et al. 2012; Lin et al. 2017; Özdemir and Hoyt 2019; Rao et al. 2016; Saini and Hoyt 2014; Shelton et al. 2015). However, a more efficient HCC management would benefit from the information about future TACE response at the time of the treatment planning phase (in which case percutaneous ablation or TARE may be opted for as an alternative). Hence, a current clinical challenge is to determine which patients will respond to TACE as effective delivery of the embolic material may be influenced by the tumor vascular supply.

We hypothesize that CEUS image-derived tumor vascular morphology features may provide predictive information for efficient TACE therapy planning and HCC patient management. Challenges for improved quantification of tumor vascular morphology in abdominal imaging include the high amount of motion artifacts that limit direct quantification of the structural information (Oezdemir et al. 2019a) and the tissue signal, i.e. clutter signal, which limits the vascular resolution reconstructed by the ultrasound (US) contrast agent (microbubble, MB)

Author Manuscript Author Manuscript Author Manuscript Author Manuscript

signal (Hoyt et al. 2015; Mauldin et al. 2011a). Another restriction is the lost visualization of small vessels in the tumor vasculature when focusing only on large vessels or vice versa during the vessel segmentation process (Oezdemir et al. 2019b). Finally, an automated image processing pipeline is useful for reproducible results and clinical translation. Herein we investigate the potential use of abdominal CEUS and advanced image processing algorithms for predicting HCC response to TACE treatment.

Materials and Methods

Ultrasound Imaging

A retrospective analysis of CEUS images of human HCC was performed ($N = 36$). Data was acquired as part of an ongoing IRB approved multi-center trial (NCT# 02764801) in which all participants provided informed consent. All US examinations were completed using a Logiq E9 scanner equipped with a C1–6-D transducer (GE Healthcare, Wauwatosa, WI). Subjects received a bolus injection of 0.2 to 0.3 ml of a MB contrast agent (Definity, Lantheus Medical Imaging, N Billerica, MA) followed by a 10 ml saline flush. CEUS imaging was performed using a dual imaging mode, enabling side-by-side visualization of the grayscale B-mode US and CEUS images at a rate of 8 to 9 frames per second. A low mechanical index (< 0.1) was used to avoid MB destruction during the US imaging sessions. A nonlinear harmonic imaging mode was used for improved MB visualization (transmit at 2 MHz, receive at 4 MHz) and gain settings were adjusted to minimize nonlinear signals prior to contrast injection. The focal zone was placed just below the approximate depth of the lesion to maximize the generation of nonlinear signals during CEUS imaging. The approximate tumor mid-line was imaged until homogenous liver enhancement was achieved (approximately 40 to 45 seconds post-injection), followed by imaging sweeps through the tumor. Patients underwent a total of three separate CEUS exams. In this study, we acquired only the pre-therapeutic baseline measurements from each subject. As a reference standard, treatment response was defined as incomplete (i.e. requiring retreatment) based on (in order of preference when available) a) pathological examination of explanted livers demonstrating live tumor; b) tumor enhancement seen with CT or MR and confirmed via angiography during retreatment; c) interval tumor growth on 6 month follow-up CE-CT/MRI; or d) asymmetrical or nodular tumor enhancement on CE-MRI/CT on 6 month follow-up. Complete treatment response was determined using pathological examination of explanted livers when available, and a complete lack of enhancement and tumor size reduction on CE-MRI/CT at 6 months in patients who did not undergo transplant. Table I shows the patient's demographics including the tumor size, location as well as the TACE treatment information. All patients were treated with a single session with CEUS data collected before retreatment was initiated.

Image Processing

A custom MATLAB (MathWorks, Inc., Natick, MA) software was developed to pre-process the images and to extract the vascular morphology features. Fig. 1 illustrates the proposed image processing and analysis pipeline. First, we applied a two-stage motion correction method to align the frames from the dynamic CEUS sequence. Following that, a singular value filter (SVF) was applied to remove the tissue signal, and a multiscale vessel

Author Manuscript Author Manuscript Author Manuscript Author Manuscript

enhancement filter was used as a pre-processing step before segmentation. After centerline detection, relevant morphological features were extracted. Finally, a distance weighted discrimination method was used to train and evaluate the vascular morphological features as TACE therapy response predictors in patients with HCC.

To delineate the tumor area, a region of interest (ROI) was drawn manually by a trained sonographer with over five years' experience in CEUS and who also conducted the US examinations. The quality of co-registered B-mode US and CEUS sequences was degraded due to patient's normal respiratory, cardiac physiology, and US transducer movement (Harput et al. 2018; Oezdemir et al. 2019a). According to the image acquisition protocol, any motion after about 40 seconds (the first 355 frames) were eliminated as the probe was rotated and resulted in out-of-plane motions. The remaining B-mode US images were used to estimate the in-plane tissue motion. Since the co-registered CEUS images contained more visible MB motion, which was relevant for the further processing steps, the tissue motion was estimated on the B-mode US image sequence. The first frame was selected as reference frame based on the assumption that the best visualization of the tumor was collected at the beginning of the acquisition. Following that, affine and non-rigid motion estimation methods were used to compute the displacements of the B-mode US images from the reference. In brief, the affine transformations compensated the global motion, and free-form deformations adjusted the motion on local regions in CEUS images using a limited memory Broyden Fletcher Goldfarb Shanno (L-BFGS) optimizer (Kroon 2011; Rueckert et al. 1999). According to the combined transformations estimated from the B-mode US images:

$$T(x, y) = T_{global}(x, y) + T_{local}(x, y) \quad (1)$$

where x and y are the pixel coordinates, the corresponding CEUS images were aligned with the reference frame (Harput et al. 2018; Oezdemir et al. 2019a).

The tissue clutter signal was removed using a SVF (Mauldin et al. 2011b). SVF is a principal component analysis (PCA) based filter using singular value decomposition (SVD). It forms a small windowed matrix over all the frames (a temporal kernel), which reduces the computation time and memory consumption for SVD. The temporal kernel helps to incorporate more local information by separating the three dominate US signals, namely, from the tissue, MB contrast agent, and noise (Demené et al. 2015). Removing the tissue artifacts from the images increases the contrast-to-tissue (CNR) ratio. After SVF, all of the frames were merged using the maximum intensity projection (MIP) technique whereby the final image has the maximum intensity values throughout consecutive frames of the image sequence at each pixel location (Forsberg et al. 2011).

To visualize the tumor vascular network in greater detail, the tubular structures of the MIP were enhanced using a multiscale vessel enhancement filter. This method has been used in magnetic resonance and computed tomography (CT) angiography to increase the diagnostic quality (Frangi et al. 1998). It uses the second fundamental form from differential geometry, which allows approximating an image locally by its second-order Taylor expansion. The first and second-order derivatives of the image in the Taylor expansion provide a directional change in intensity values and curvature information of the image (Gonzalez and Woods

Author Manuscript Author Manuscript Author Manuscript Author Manuscript

2018). Specifically, the eigenvectors of the Hessian matrix give the amount of intensity variations. Tubular structures are detected as structures with high variations in the longitudinal direction and low variations in cross-sectional direction, *i.e.*, the highest eigenvalues and its orthogonal counterpart at each pixel, respectively. Derivatives of the image are provided by the convolutions with the derivatives of Gaussian kernels, while multiscale enhancement is achieved by different sigma (the width of the kernel) values of these Gaussians. A vesselness function $V_o(\gamma)$ results in higher values for tubular structures in 2D and minimizes the noise:

$$V_o(\gamma) = \begin{cases} 0 & \text{if } \lambda_2 > 0 \\ exp\left(-\frac{R_B 2}{2\beta^2}\right)\left(1 - exp\left(-\frac{s^2}{2c^2}\right)\right) \end{cases} \quad (2)$$

$$R_B = \frac{|\lambda_1|}{\sqrt{|\lambda_2|}}, S = \sqrt{\sum_{j=1}^{2} \lambda_j^2}$$

where $\lambda_{1,2}$ are eigenvalues from the Hessian matrix of the image, R_B is for identification of blob-like or tubular patterns, S is the definition of the structureness, γ is used for the different scales of Gaussian kernels, β and c are the regularization parameters for adjusting filter sensitivity. With this, thicker vessels are detected by kernels with a large sigma, while thinner vessels are detected by kernels with a small sigma in the scale selection process.

Using the same clinical US system and settings used for patient data collection, a flow phantom of known vessel dimensions was used to calibrate the custom software for the scale range selection in a controlled environment. Although this scale selection process can be optimized for thicker vessels, finding a lower bound for the thinner vessels was only possible with the risk of including some noise or removing some desired vessel signal. Hence, this lower limit was assessed qualitatively by the amount of background suppression. After the scale selection process, a multiscale image with enhanced vascular structures was created.

Morphological Feature Extraction

To use morphological image operations, vessels from the multiscale image were segmented using an adaptive thresholding method (Bradley and Roth 2007). This method first creates an integral image to compute the average value of the neighboring pixels. The binary image is created by the comparison of the current pixel value with this average. The foreground and background pixels from the binary image were used to compute the morphological features of tumor vasculature. First, the vessel-to-tissue ratio (VR) was estimated (Hoyt et al. 2015).

The centerlines of the segmented vessels were extracted using a parallel thinning algorithm (Zhang and Suen 1984) as a simplified version of the tumor vascular network. This method keeps the same digital connectivity patterns and the topology of the vascular structures by modifying 8-connected skeletons and retaining diagonal lines as well as 2 × 2 squares (Lam et al. 1992). As shown in Fig. 2, the nodes and edges of the skeletonized network was considered as bifurcations (or branching points) and individual vessel segments,

Author Manuscript Author Manuscript Author Manuscript Author Manuscript

respectively. Accordingly, the number of bifurcations (NB) was found by counting each node of the network, and the number of vessels (NV) was the edge count of the network. As introduced in our previous work (Özdemir and Hoyt 2019), the distance transform was used to estimate vessel diameters at each pixel on the centerline as the Euclidian distance between the centerline pixel and the closest edge pixel of the regarded tubular structure (vessel edge). A mean vessel diameter for the entire tumor was then computed by averaging all of the mean diameters from individual vessel segments. Similarly, the mean vessel length (VL) and vessel tortuosity (VT) metrics were computed by averaging over all of the vessel segments (Hoyt et al. 2015). Note VT as metric value is zero only for straight vessel segments.

Feature Selection and Model Assessment

The predictability of HCC response to TACE treatment was evaluated using a distance weighted discrimination method (DWD) (Marron et al. 2007). This employs an improved machine learning method for statistical analysis of high-dimension low-sample size data. Similar to support vector machines (SVM), DWD discriminates the data into two classes but different from SVM; DWD avoids data piling and increases the generalizability of the model. The small sample size of our dataset is the rationale of choosing the DWD as the classification algorithm.

All of the data points were labeled with one of the two classes, i.e., complete and incomplete response to prepare the training data (James et al. 2013). The leave one out cross-validation method was used to have a reliable accuracy (Hastie et al. 2009). For this, the sample (N = 36) was divided into a construction (N = 35) and a validation (N = 1) sub-datasets for each patient data (Stone 1974). Thus, 36 different models were trained separately with 35 patient's data and validated on one exam. In the end, the average accuracy of all 36 cases was reported as the final accuracy. To investigate the contributions of the six extracted features from tumor vasculature for the prediction of the TACE response, two models were trained with a different set of features. The first model used all of the features, while the second model used only the most discriminative features, which was assessed visually by the pair plots of features, i.e. the most correlated features were excluded. Both models were tuned using a polynomial kernel with different values for the hyper-parameters and the best performing model was chosen from the largest values of accuracy and interrater reliability statistics (kappa). The data were centered and scaled in a pre-processing step before each training. All computations and data analyses were performed using a statistical software package (R Foundation for Statistical Computing, Vienna, Austria) (Kuhn 2008; R core team 2013).

Results

CEUS image-derived vascular morphological features were used to evaluate HCC response to TACE treatment in 36 patients. According to the CT, MRI, and pathology outcomes, 19 patients had a complete response, and the other 17 had an incomplete response. Fig. 3 shows the two-step motion correction results using two representative patients' data with complete and incomplete response, respectively. Starting from a single B-mode US image showing the anatomical structures, two MIPs of the initial dynamic B-mode US and CEUS image

Author Manuscript Author Manuscript Author Manuscript Author Manuscript

sequence have a challenging view of the tumor. Because MIPs are created using the maximum intensity value of each frame for each pixel location. Thus, the MIPs without any filtering have intensity saturations, e.g. bright pixels. Here, the raw results after MIP step were presented directly without any gain compensation for a comparison with the results after motion correction process. After the correction of the in-plane motion, the abdominal structures and the tumor vasculature are more visible in the MIP. These representative US images demonstrate the need for motion correction in the image processing pipeline to improve tumor visibility before starting with the feature extraction.

The effect of clutter signal removal is illustrated in Fig. 4. The presence of the tissue signal can complicate vessel detection. Removing the tissue signal increased the CNR as depicted in the paired images. These SVF outputs improve the results of the multiscale vessel enhancement filter in the next step. The morphological image processing results summarized in three steps for each of the representative cases, is depicted in Fig. 5. First, the results from the multiscale vessel enhancement filter is overlaid on the SVF results. The enlarged ROIs depict the binary image before spatial morphological filters like opening and closing. The enlarged ROIs also represent the centerlines detected from the binary vasculature. The simplified tumor network topology (centerlines) indicates the vascular routes for effective drug delivery, which is crucial for effective embolization. Fig. 6 and Fig. 7 present cases of HCC from individual patients for complete responders and incomplete responders, respectively. The colors indicate the vessel diameters. Here, the difference in tumor vascular complexity for the complete and incomplete response groups can be assessed qualitatively. A larger number of vessels and bifurcations contribute more to the chaotic visualizations of the tumor vascular networks which was observed more in incomplete responders group.

CEUS derived morphological features were used to assess the correlated and discriminative features qualitatively for complete and incomplete response patients. As highlighted in Fig. 8, the weakest feature was the VD parameter compared to all other features. Training with all of the features achieved only a 52% accuracy while training with the feature set where VD was excluded achieved an accuracy of 72% and training with the dominant features (NV, NB, and VR) achieved the best overall accuracy of 86%. As informed by the pair plot and confirmed by the accuracy, the dominant features, namely, NV, NB, and VR, were selected to train and tune the final machine learning model. As listed in Table II, this final model achieved a validation accuracy of 86% (95% CI [0.70, 0.95]) and a kappa statistic of 72%. A sensitivity and specificity of 89% and 82%, respectively, were obtained. Table III details the confusion matrix for the model performance in terms of individual predictions. Overall, these performance metrics showed that our model was able to make reliable pre-therapeutic HCC response to TACE predictions.

Discussion

The strength of the proposed image processing and analysis method is that it is based on the patient specific geometry of their tumor vascular network while addressing the image processing challenges, such as motion artifacts, tissue signal, and multi-scale segmentation in abdominal CEUS imaging before parameterization. This enables automated pre-processing for each patient and a reliable prediction of the TACE therapy response.

Author Manuscript Author Manuscript Author Manuscript Author Manuscript

Reproducible quantifications of HCC vascular networks depicted in CEUS images and the prediction of pre-therapeutic TACE response, can improve customized treatment strategies in personalized medicine.

Aggressive tumors are known to have chaotic angiogenic networks (Weidner et al. 1991) with more tortuous (Gessner et al. 2012; Lin et al. 2017; Rao et al. 2016) and dense vasculature (Hoyt et al. 2015). The complexity of the tumor vascular network may affect the arterial delivery of the drug-eluting beads during TACE treatment. Thus, quantification of the tumor angiogenic network may provide crucial information for physicians during treatment planning. The NV, NB and VR parameters were shown to be the most effective features for predicting HCC response to TACE. The more bifurcations in the angiogenic network may result in more embolization targets.

If it is believed that the intra-arterial therapies will not provide adequate treatment response, alternative locoregional therapies such as ablation or radiation may be employed. In this study, CEUS image-derived morphological features of the HCC vascular network were able to predict the eventual TACE response. The preliminary results indicate that liver tumors with less complex vascular networks have a higher potential for a complete response to TACE therapy. This may be partially attributed to the fact that tumors with more developed vascular patterns may have multiple feeding sources, requiring multiple TACE treatments for complete embolization. These tumors may be more amenable to TARE, which requires localized deposit of radiation containing beads but not complete embolization of the tumor vasculature.

Using MRI as a preoperative conventional, image features and texture analysis have been shown to predict tumor response to TACE treatment (Zhang et al. 2019). Texture features from CT images have also been shown to be potential predictors for identifying patients who are not suitable for TACE treatment (Cai et al. 2019; Park et al. 2017; Yu et al. 2018). In a more recent study, it was shown that CT-derived image features can predict the response of TACE using a residual convolutional neural network with up to 85% accuracy (Peng et al. 2020). Another recent study aimed to establish the feasibility of an artificial intelligence–based radiomics strategy for predicting TACE response (Liu et al. 2020). To date none of these approaches have resulted in clinical adoption.

CEUS imaging can be used to help monitor tumor response to systemic drug treatment (Hoyt et al. 2015; Nam et al. 2018). Advanced image analysis of breast tumor vascular networks depicted in clinical CEUS images showed both a strong correlation between functional and structural tumor parameters as well as to the post-therapeutic monitoring capabilities of CEUS image-derived morphological features (Hoyt et al. 2015). This study introduced a method for quantification of unique vascular morphological features while the motion artifacts caused by patient, organ, or transducer motion were neglected during the image processing. Motion artifacts can negatively impact the accuracy during quantification of vascular morphological features. In a recent preclinical study, a simpler morphological feature called the vascular network length was used (Theek et al. 2018). This parameter was shown to be a feasible metric for describing tumor vascular morphology from CEUS images with the support of the other features, such as first- order statistics, functional, textural, and

Author Manuscript Author Manuscript Author Manuscript Author Manuscript

wavelet-based features. This study segmented the tumor vasculature by intensity thresholding without addressing the potential lost visualization of the smaller vessels when focused on larger vessels only. Segmentation at only one scale can also affect the quantification of vascular morphology. Our method addressed both of these challenges and helped improve the overall CEUS image quantification process.

Showing the feasibility of morphological feature extraction from HCC tumor vasculature and the ability of assessing the future TACE response, this study is limited by its small sample size. Before introducing to the clinical practice, the approach presented in this paper needs to be extensively validated using a large sample size and data from different sites.

Conclusion

A novel CEUS image processing and analysis method was developed that both extracts the morphological features from the tumor vascular network and predicts HCC response to TACE treatment. Introduction of a reliable method for predicting a TACE response may help provide more effective therapeutic planning and more personalized patient strategies.

Acknowledgements

This work was supported in part by National Institutes of Health (NIH) R01CA194307, R01EB025841, and Cancer Prevention Research Institute of Texas (CPIRIT) grant RP180670. GE Healthcare provided equipment support and Lantheus Medical Imaging provided the Definity. Texas Advanced Computing Center (TACC) at the University of Texas at Austin for providing HPC resources that have contributed to the research results reported within this paper.

References

Altekruse SF, McGlynn KA, Reichman ME. Hepatocellular carcinoma incidence, mortality, and survival trends in the United States from 1975 to 2005. J Clin Oncol 2009;27:1485–1491. [PubMed: 19224838]

Averkiou MA, Bruce MF, Powers JE, Sheeran PS, Burns PN. Imaging methods for ultrasound contrast agents. Ultrasound in Medicine & Biology 2020;46:498–517. [PubMed: 31813583]

Bradley D, Roth G. G.: Adaptive thresholding using the integral image. ACM J Graph Tools 2007;13–21.

Brown DB, Nikolic B, Covey AM, Nutting CW, Saad WEA, Salem R, Sofocleous CT, Sze DY. Quality improvement guidelines for transhepatic arterial chemoembolization, embolization, and chemotherapeutic infusion for hepatic malignancy. Journal of Vascular and Interventional Radiology 2012;23:287–294. [PubMed: 22284821]

Cai Q, Mao Y, Yang Q, Wen H, Li S, Zhang R. Texture analysis of computed tomography images for predicting the efficacy of transcatheter arterial chemoembolization in hepatocellular carcinoma patients. Rochester, NY: Social Science Research Network, 2019 3 Report No.: ID 3356855.

Demené C, Deffieux T, Pernot M, Osmanski BF, Biran V, Gennisson JL, Sieu LA, Bergel A, Franqui S, Correas JM, Cohen I, Baud O, Tanter M. Spatiotemporal clutter filtering of ultrafast ultrasound data highly increases doppler and fultrasound sensitivity. IEEE Transactions on Medical Imaging 2015;34:2271–2285. [PubMed: 25955583]

Eisenbrey JR, Joshi N, Dave JK, Forsberg F. Assessing algorithms for defining vascular architecture in subharmonic images of breast lesions. Physics in Medicine and Biology 2011;56:919–930. [PubMed: 21248388]

Forsberg F, Ro RJ, Fox TB, Liu J-B, Chiou S-Y, Potoczek M, Goldberg BB. Contrast enhanced maximum intensity projection ultrasound imaging for assessing angiogenesis in murine glioma and breast tumor models: A comparative study. Ultrasonics 2011;51:382–389. [PubMed: 21144542]

Author Manuscript Author Manuscript Author Manuscript Author Manuscript

Frangi AF, Niessen WJ, Vincken KL, Viergever MA. Multiscale vessel enhancement filtering. SpringerLink Springer, Berlin, Heidelberg, 1998 pp. 130–137.

Gessner RC, Aylward SR, Dayton PA. Mapping microvasculature with acoustic angiography yields quantifiable differences between healthy and tumor-bearing tissue volumes in a rodent model. Radiology 2012;264:733–740. [PubMed: 22771882]

Ghosh D, Peng J, Brown K, Sirsi S, Mineo C, Shaul PW, Hoyt K. Super-resolution ultrasound imaging of skeletal muscle microvascular dysfunction in an animal model of type 2 diabetes. J Ultrasound Med 2019;38:2589–2599. [PubMed: 30706511]

Gonzalez RC, Woods RE. Digital Image Processing. 4th ed. New York, NY, USA: Pearson, 2018.

Harput S, Christensen-Jeffries K, Brown J, Li Y, Williams KJ, Davies AH, Eckersley RJ, Dunsby C, Tang MX. Two-stage motion correction for super-resolution ultrasound imaging in human lower limb. IEEE Transactions on Ultrasonics, Ferroelectrics, and Frequency Control 2018;65:803– 814.

Hastie T, Tibshirani R, Friedman J. The elements of statistical learning. 2nd ed. New York, NY, USA: Springer-Verlag, 2009.

Hoyt K, Sorace A, Saini R. Quantitative mapping of tumor vascularity using volumetric contrast enhanced ultrasound. Invest Radiol 2012;47:167–174. [PubMed: 22104962]

Hoyt K, Umphrey H, Lockhart M, Robbin M, Forero-Torres A. Ultrasound imaging of breast tumor perfusion and neovascular morphology. Ultrasound Med Biol 2015;41:2292–2302. [PubMed: 26116159]

James G, Witten D, Hastie T, Tibshirani R. An introduction to statistical learning. 1st ed. New York, NY, USA: Springer-Verlag, 2013.

Kim H, El-Serag HB. The epidemiology of hepatocellular carcinoma in the usa. Curr Gastroenterol Rep 2019;21:17. [PubMed: 30976932]

Kloeckner R, Otto G, Biesterfeld S, Oberholzer K, Dueber C, Pitton MB. Mdct versus mri assessment of tumor response after transarterial chemoembolization for the treatment of hepatocellular carcinoma. Cardiovasc Intervent Radiol 2010;33:532–540. [PubMed: 19847482]

Kroon DJ. B-spline Grid, Image and Point based Registration. Mathworks 2011;

Kuhn M Building predictive models in r using the caret package. Journal of Statistical Software 2008;28:1–26. [PubMed: 27774042]

Lam L, Lee S-W, Suen CY. Thinning methodologies-a comprehensive survey. IEEE Transactions on Pattern Analysis and Machine Intelligence 1992;14:869–885.

Lin F, Shelton SE, Espíndola D, Rojas JD, Pinton G, Dayton PA. 3-d ultrasound localization microscopy for identifying microvascular morphology features of tumor angiogenesis at a resolution beyond the diffraction limit of conventional ultrasound. Theranostics 2017;7:196–204. [PubMed: 28042327]

Liu D, Liu F, Xie X, Su L, Liu M, Xie X, Kuang M, Huang G, Wang Y, Zhou H, Wang K, Lin M, Tian J. Accurate prediction of responses to transarterial chemoembolization for patients with hepatocellular carcinoma by using artificial intelligence in contrast-enhanced ultrasound. Eur Radiol 2020;

Marron JS, Todd MJ, Ahn J. Distance-Weighted Discrimination. Journal of the American Statistical Association 2007;102:1267–1271.

Mauldin FW, Lin D, Hossack JA. The Singular Value Filter: A General Filter Design Strategy for PCA-Based Signal Separation in Medical Ultrasound Imaging. IEEE Trans Med Imaging 2011a;30:1951–1964. [PubMed: 21693416]

Mauldin FW, Lin D, Hossack JA. The Singular Value Filter: A General Filter Design Strategy for PCA-Based Signal Separation in Medical Ultrasound Imaging. IEEE Transactions on Medical Imaging 2011b;30:1951–1964. [PubMed: 21693416]

Nam K, Stanczak M, Lyshchik A, Machado P, Kono Y, Forsberg F, Shaw CM, Eisenbrey JR. Evaluation of hepatocellular carcinoma transarterial chemoembolization using quantitative analysis of 2d and 3d real-time contrast enhanced ultrasound. Biomedical Physics & Engineering Express 2018;4:035039.

Oezdemir I, Shaw C, Eisenbrey JR, Hoyt K. Improved quantitative contrast-enhanced ultrasound imaging of hepatocellular carcinoma response to transarterial chemoembolization. IEEE 16th International Symposium on Biomedical Imaging (ISBI 2019) 2019a;:1737–1740.

Author Manuscript Author Manuscript Author Manuscript Author Manuscript

Oezdemir I, Wessner CE, Shaw C, Eisenbrey JR, Hoyt K. Multiscale quantification of tumor microarchitecture for predicting therapy response using dynamic contrast-enhanced ultrasound imaging. IEEE International Ultrasonics Symposium (IUS) 2019b;:1173–1176.

Özdemir I, Hoyt K. Morphological processing for multiscale analysis of super-resolution ultrasound images of tissue microvascular networks. Medical Imaging: Ultrasonic Imaging and Tomography 2019;10955:1095505.

Park HJ, Kim JH, Choi S, Lee ES, Park SJ, Byun JY, Choi BI. Prediction of therapeutic response of hepatocellular carcinoma to transcatheter arterial chemoembolization based on pretherapeutic dynamic ct and textural findings. American Journal of Roentgenology 2017;209:W211–W220. [PubMed: 28813195]

Peng J, Kang S, Ning Z, Deng H, Shen J, Xu Y, Zhang J, Zhao W, Li X, Gong W, Huang J, Liu L. Residual convolutional neural network for predicting response of transarterial chemoembolization in hepatocellular carcinoma from CT imaging. Eur Radiol 2020;30:413–424.

R core team. R: The R project for statistical computing. 2013.

Rao SR, Shelton SE, Dayton PA. The “fingerprint” of cancer extends beyond solid tumor boundaries: assessment with a novel ultrasound imaging approach. IEEE Transactions on Biomedical Engineering 2016;63:1082–1086. [PubMed: 26394410]

Rueckert D, Sonoda LI, Hayes C, Hill DLG, Leach MO, Hawkes DJ. Nonrigid registration using free-form deformations: application to breast MR images. IEEE Transactions on Medical Imaging 1999;18:712–721. [PubMed: 10534053]

Saini R, Hoyt K. Recent developments in dynamic contrast-enhanced ultrasound imaging of tumor angiogenesis. Imaging Med 2014;6:41–52. [PubMed: 25221623]

Shaw CM, Eisenbrey JR, Lyshchik A, O’Kane PL, Merton DA, Machado P, Pino L, Brown DB, Forsberg F. Contrast-enhanced ultrasound evaluation of residual blood flow to hepatocellular carcinoma after treatment with transarterial chemoembolization using drug-eluting beads. Journal of Ultrasound in Medicine 2015;34:859–867. [PubMed: 25911704]

Shelton SE, Lee YZ, Lee M, Cherin E, Foster FS, Aylward SR, Dayton PA. Quantification of microvascular tortuosity during tumor evolution using acoustic angiography. Ultrasound in Medicine & Biology 2015;41:1896–1904.

Stone M Cross-validatory choice and assessment of statistical predictions. Journal of the Royal Statistical Society Series B (Methodological) 1974;36:111–147.

Theek B, Opacic T, Magnuska Z, Lammers T, Kiessling F. Radiomic analysis of contrast-enhanced ultrasound data. Sci Rep 2018 [cited 2020 Jan 8];8. Available from: https://www.ncbi.nlm.nih.gov/pmc/articles/PMC6063906/

Weidner N, Semple JP, Welch WR, Folkman J. Tumor angiogenesis and metastasis — correlation in invasive breast carcinoma. New England Journal of Medicine 1991;324:1–8.

Yamada R, Kishi K, Sato M, Sonomura T, Nishida N, Tanaka K, Shioyama Y, Terada M, Kimura M. Transcatheter arterial chemoembolization (tace) in the treatment of unresectable liver cancer. World J Surg 1995;19:795–800. [PubMed: 8553668]

Yan F-H, Zhou K-R, Cheng J-M, Wang J-H, Yan Z-P, Da R-R, Fan J, Ji Y. Role and limitation of fmpspgr dynamic contrast scanning in the follow-up of patients with hepatocellular carcinoma treated by tace. World J Gastroenterol 2002;8:658–662. [PubMed: 12174374]

Yu JY, Zhang HP, Tang ZY, Zhou J, He XJ, Liu YY, Liu XJ, Guo DJ. Value of texture analysis based on enhanced mri for predicting an early therapeutic response to transcatheter arterial chemoembolisation combined with high-intensity focused ultrasound treatment in hepatocellular carcinoma. Clinical Radiology 2018;73:758e9–758.e18.

Zhang H, He X, Yu J, Song W, Liu X, Liu Y, Zhou J, Guo D. Preoperative mri features and clinical laboratory indicators for predicting the early therapeutic response of hepatocellular carcinoma to transcatheter arterial chemoembolization combined with high-intensity focused ultrasound treatment. BJR 2019;92:20190073. [PubMed: 31166700]

Zhang TY, Suen CY. A fast parallel algorithm for image processing and computer vision. 1984;27:4.

Author Manuscript Author Manuscript Author Manuscript Author Manuscript

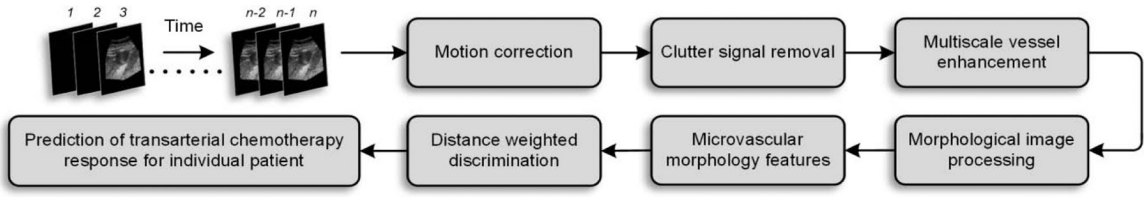

Figure 1:

Image processing and analysis pipeline for prediction of transarterial chemotherapy (TACE) response for an individual patient with hepatocellular carcinoma (HCC). The contrast-enhanced ultrasound (CEUS) image sequence was aligned using the first frame as reference. Tissue signal was removed, and vasculature was enhanced at multiple scales before segmentation. Using morphological operations, tumor microvascular features were extracted. A distance-weighted discriminator was trained using the CEUS image-derived morphological features and leave-one-out validation.

Author Manuscript Author Manuscript Author Manuscript Author Manuscript

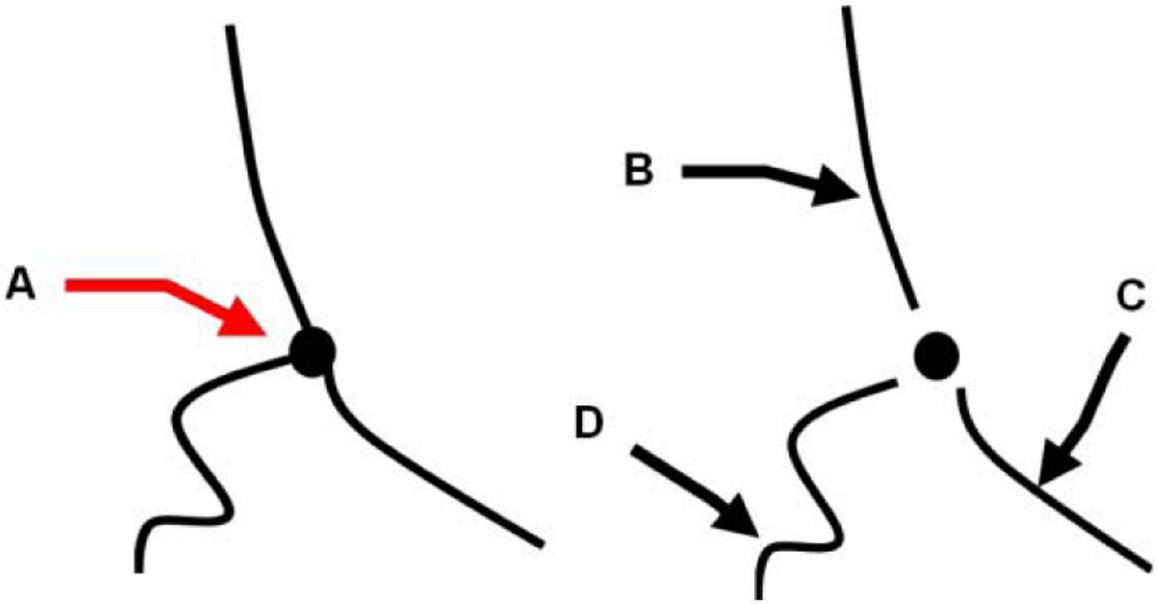

Figure 2:

Schematic for the definition of select morphological features. The simplified tumor angiogenic network from centerlines of the tubular structures contain vessels with branching points or nodes (A). Individual vessel segments, edges are counted after the removal of the branching point. (B), (C), and (D) denote individual vessels with gradually increased tortuosity and different vessel length.

Author Manuscript Author Manuscript Author Manuscript Author Manuscript

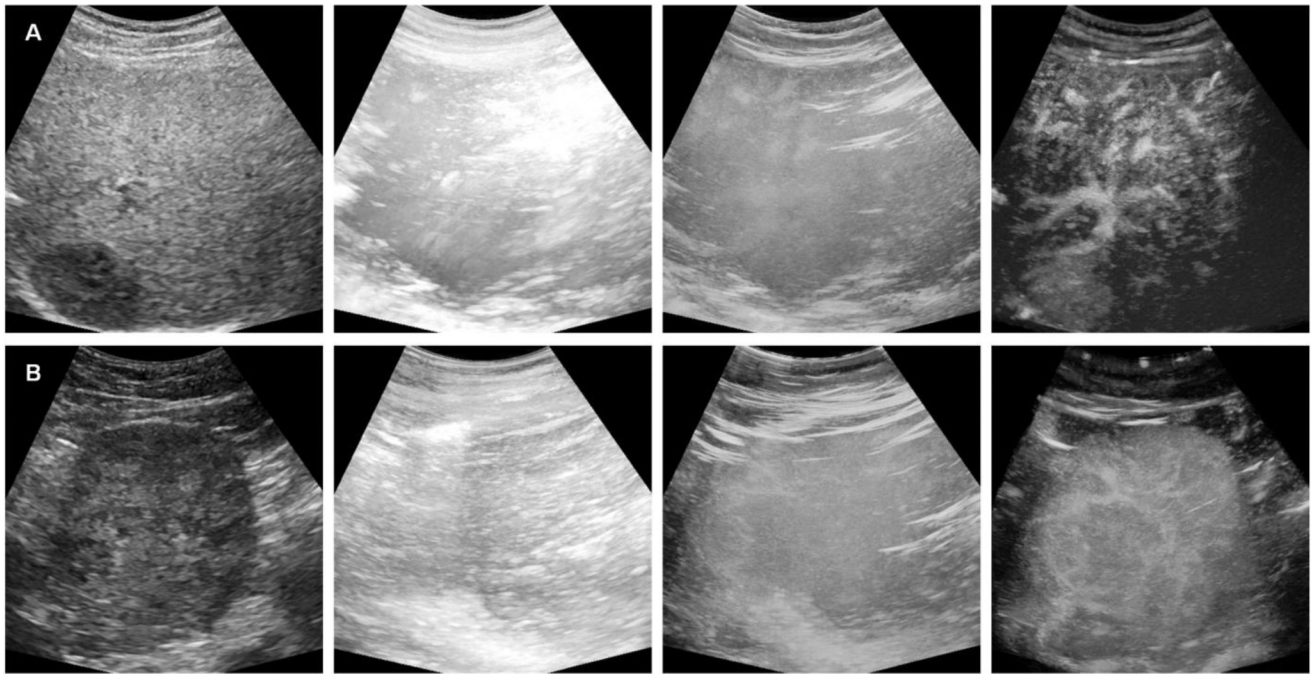

Figure 3:

Representative ultrasound (US) results from patients with HCC determined to have either a complete (top) or incomplete (bottom) response to TACE treatment. As shown from left to right are the B-mode US image, maximum intensity projection (MIP) of the original B-mode US, CEUS image, and MIP of the motion corrected CEUS image sequence.

Author Manuscript Author Manuscript Author Manuscript Author Manuscript

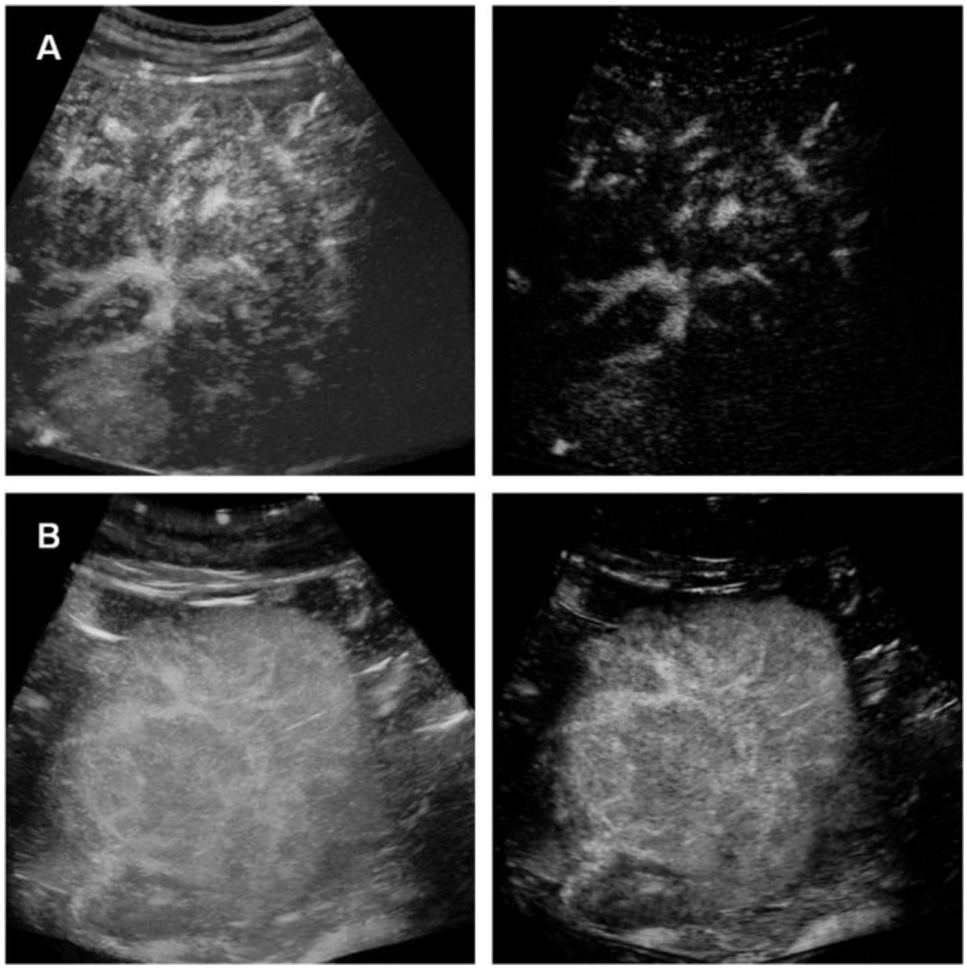

Figure 4:
Representative results after spatiotemporal filtering of the CEUS images from patients with HCC determined to have either a complete (top) or incomplete (bottom) response to TACE treatment.

Author Manuscript Author Manuscript Author Manuscript Author Manuscript

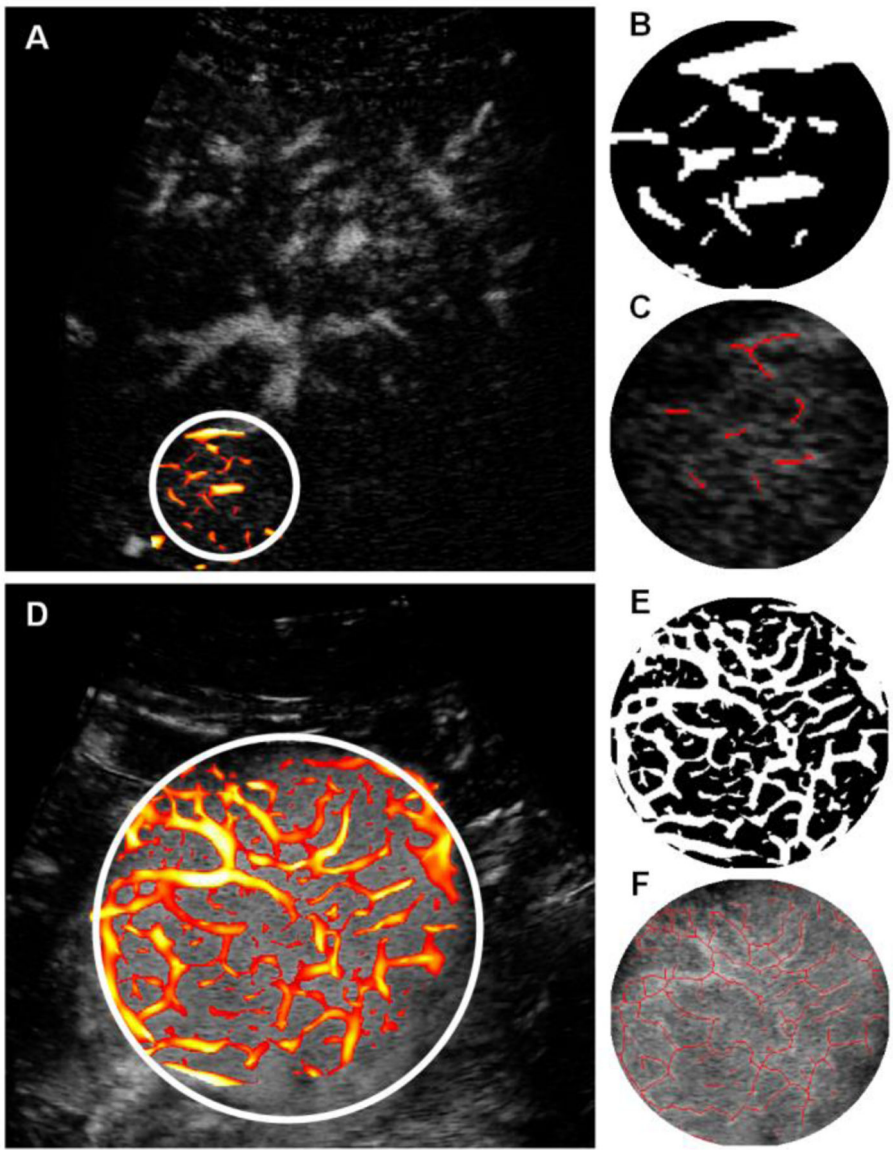

Figure 5:
Morphological operations after application of multiscale vessel enhancement in (A) and (D), the result of spatial filtering and binarization in (B) and (E) , and the centerline detection in (C) and (F) for the representative complete and incomplete response patients, respectively.

Author Manuscript Author Manuscript Author Manuscript Author Manuscript

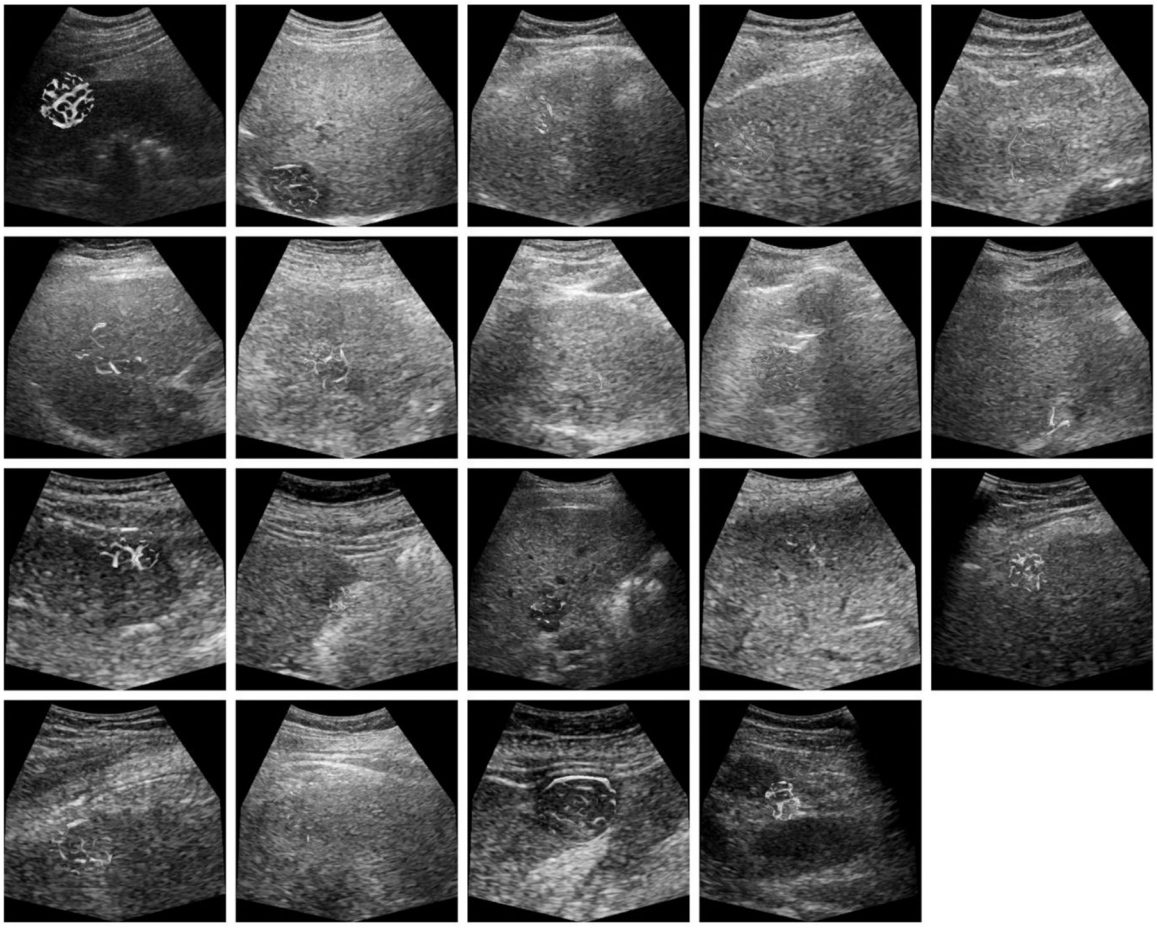

Figure 6:
US images from patients with HCC that exhibited a complete response to TACE treatment. Microvascular morphological structures are overlaid on a single B-mode US image (reference frame). Color indicates the vessel diameter measurements from red (high) to blue (low).

Author Manuscript Author Manuscript Author Manuscript Author Manuscript

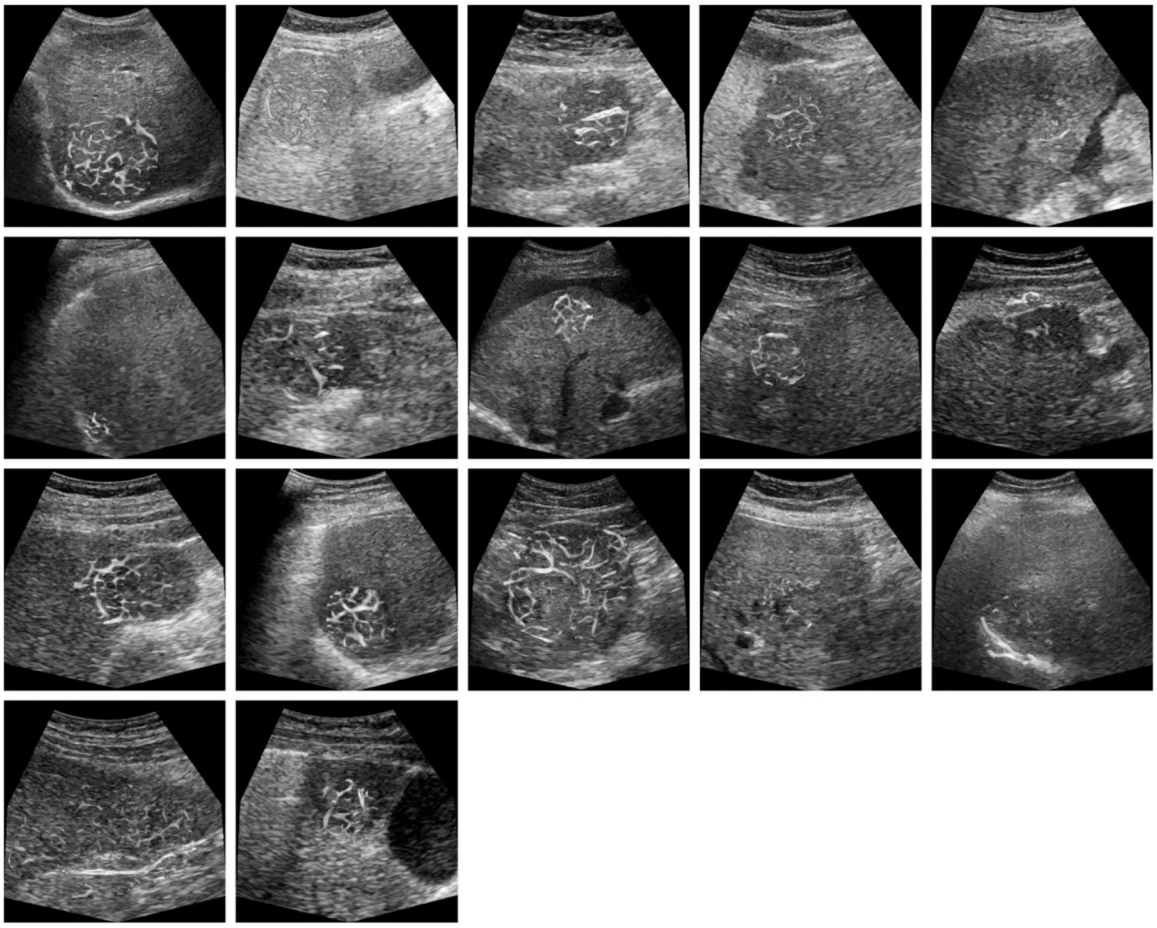

Figure 7:
US images from patients with HCC that exhibited an incomplete response to TACE treatment. Microvascular morphological structures are overlaid on a single B-mode US image. Color indicates the vessel diameter measurements from red (high) to blue (low). Note that tumors are relatively large and have a more chaotic microvascular structure compared to patient tumors that exhibit a complete response to TACE.

Author Manuscript Author Manuscript Author Manuscript Author Manuscript

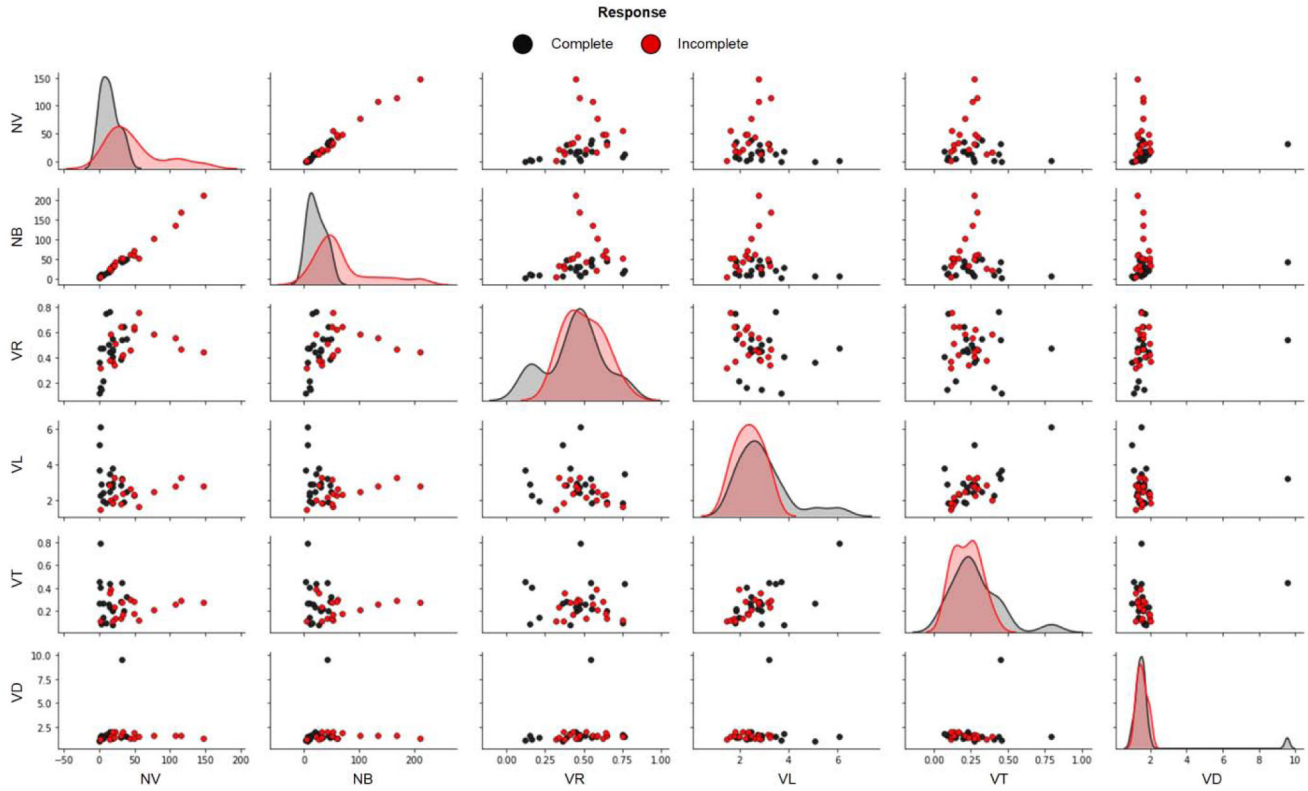

Figure 8:

Visual assessment of morphological features from patients that were determined to have undergone either a complete or incomplete response TACE. Number of vessels (NV), number of branching points (NB), vessel-to-tissue ratio (VR), mean vessel length (VL), mean vessel tortuosity (VT), and mean vessel diameter (VD).

Author Manuscript Author Manuscript Author Manuscript Author Manuscript

TABLE I.

PATIENT INFO: SEX, BODY MASS INDEX (BMI), AGE, TUMOR DIMENSION, TUMOR LOCATION, RECEIVED TREATMENT (LIPIODOL(C-TACE) VS. DEBBOX)), AND TRANSARTERIAL CHEMOEMBOLIZATION (TACE) RESPONSE RESULTS

Subject number	Sex	BMI (kg/m^2)	Age	Largest tumor dimension (cm)	Tumor location	Received treatment	TACE response
1	M	35.3	63	2.0	S.gm.6	c-TACE	Complete
2	M	22.1	71	7.1	Segm ent7	c-TACE	Incomplete
3	M	21.0	52	4.2	Segment 8	DEB-TACE	Complete
4	M	39.2	44	2.4	Segment 8	c-TACE	Complete
5	M	31.9	68	2.3	Segment 7	DEB-TACE	Complete
6	M	28.1	62	_.°	Segment 2	c-TACE	Complete
7	M	41.8	42	5.5	Segment 4	DEB-TACE	Incomplete
8	M	24.0	48	4.0	Segment 3	DEB-TACE	Incomplete
9	M	30.0	69	4.1	Segment 2	DEB-TACE	Incomplete
10	F	27.3	47	2.5	Segment 5	DEB-TACE	Incomplete
11	M	26.5	70	18	Segment 7	DEB-TACE	Incomplete
12	M	33.2	60	2.4	Segment 8	DEB-TACE	Complete
13	M	23.7	67	2.8	Segment 6	DEB-TACE	Incomplete
14	M	27.3	8	2.4	Segment 8	DEB-TACE	Complete
15	M	27.5	62	2.1	Segment 2 / 3	DEB-TACE	Complete
16	F	37.7	,4	2.5	Segment 7	DEB-TACE	Complete
17	M	29.0	56	2.6	Segment 2	DEB-TACE	Complete
18	M	‘4.0	56	1.8	Segment 3	DEB-TACE + c-TACE	Complete
19	M	23.9	54	3.0	Segment 8	DEB-TACE + c-TACE	Incomplete
20	M	28.7	67	2.6	Segment 4A	c-TACE	Incomplete
21	M	26.2	69	6.3	Segment 8	DEB-TACE + c-TACE	Incomplete
22	M	29.5	65	1.5	Segment 6	DEB-TACE + c-TACE	Complete
23	M	NA	62	3.5	Segment 6	DEB-TACE	Complete
24	M	19.7	56	NA	Segment 2	DEB-TACE + c-TACE	Complete
25	M	25.9	66	3.8	Segment 5	DEB-TACE	Incomplete
26	F	22.4	72	5.9	Segment 7	DEB-TACE + c-TACE	Incomplete
27	M	31.4	60	8.1	Segment 2	DEB-TACE	Incomplete
28	F	27.7	71	3.8	Segment 4	DEB-TACE	Incomplete
29	M	31.9	74	2.4	Segment 8	DEB-TACE + c-TACE	Complete
30	M	25.8	66	1.3	Segment 8	DEB-TACE + c-TACE	Complete
31	M	39.0	72	7.2	Segment 7	DEB-TACE + c-TACE	Incomplete
32	M	23.9	69	8.4	Segment 6	DEB-TACE + c-TACE	Incomplete
33	M	31.0	64	2.9	Segment 6	DEB-TACE + c-TACE	Complete
34	F	NA	65	2.8	Segment 4B	DEB-TACE	Complete
35	M	25.0	66	1.7	Segment 8	c-TACE	Complete
36	F	32.0	62	3.0	Segment 8	DEB-TACE	Incomplete

Author Manuscript

Author Manuscript

Author Manuscript

Author Manuscript

TABLE II.

MODEL PERFORMANCE METRICS

Model Trained with Features	NV, NB, and VR
Accuracy	86 %
Kappa	72 %
Sensitivity	89 %
Specifity	82 %
%95 CI*	0.705 – 0.953

* CI = Confidence Interval

NV = Number of vessels, NB = Number of bifurcations,

VR = Vessel-to-tissue ratio

Author Manuscript

Author Manuscript

Author Manuscript

Author Manuscript

TABLE III.

LEAVE-ONE-OUT CROSS-VALIDATION RESULTS

Predictions/True Response	Incomplete	Complete
Incomplete	14	2
Complete	3	17